Journal of Biomechanics 74 (2018) 156–162

Contents lists available at ScienceDirect

Journal of Biomechanics

journal homepage: www.elsevier.com/locate/jbiomech
www.JBiomech.com

Biomechanical characterization of the native porcine aortic root

T. Bechsgaard [a,b,c,1], T. Lindskow [b,c,1], T. Lading [b,c], J.M. Hasenkam [b,c,*], D.M. Røpcke [b,c], H. Nygaard [b,c], P. Johansen [a,b,c], S. L. Nielsen [b,c]

[a] Department of Engineering, Faculty of Science and Technology, Aarhus University, Finlandsgade 22, 8200 Aarhus N, Denmark
[b] Department of Cardiothoracic and Vascular Surgery, Aarhus University Hospital, Palle Juul-Jensens Boulevard 99, 8200 Aarhus N, Denmark
[c] Department of Clinical Medicine, Aarhus University Hospital, Palle Juul-Jensens Boulevard 99, 8200 Aarhus N, Denmark

ARTICLE INFO

Article history:
Accepted 22 April 2018

Keywords:
Force measurements
Biomechanical characterization
Geometrical analysis
Segmental analysis

ABSTRACT

A thorough understanding of the well-functioning, native aortic root is pivotal in an era, where valve sparing surgical techniques are developed and used with increasing frequency. The objective of this study was to characterize the local structural stiffness of the native aortic root, to create a baseline for understanding how different surgical interventions affect the dynamics of the aortic root. In this acute porcine study (N = 10), two dedicated force transducers were implanted to quantify the forces acting on both the annular plane and on the sinotubular junction (STJ). To assess the changes in geometry, eleven sonomicrometry crystals were implanted within the aortic root. The combination of force and length measurements yields the radial structural stiffness for each segment of the aortic root.

The least compliant segment at the annular plane was the right-left interleaflet triangle with a stiffness modulus of 1.1 N mm^{-1} (SD0.4). At the sinotubular junction the same segment (right-left) was most compliant, compared with the two other segments, however not statistically significant different.

The elastic energy storage was derived from the aortic root pressure volume relationship; the mean elastic energy storage was 826 μJ (SD529). In conclusion, the aortic root has been characterized in terms of both segmental forces, segmental change in length and elastic energy storage. This study is the first to assess the radial structural stiffness of different segments of the aortic root. The presented data is reference for further studies regarding the impact of surgical interventions on the aortic root.

1. Introduction

The preferred method for treating patients with aortic valve insufficiency, both with and without aortic root pathology, has been replacement of the native valve with a prosthetic valve. As surgical techniques have improved, valve sparing repair procedures (David and Feindel, 1992; Sarsam and Yacoub, 1993) have become attractive alternatives to aortic valve replacement (Boodhwani and El Khoury, 2014). A prerequisite for a durable repair is an in-depth understanding of the interaction between the aortic valve leaflets and the functional aortic annulus that comprises the ventricular-aortic junction (annulus) and sino-tubular junction (STJ) (de Kerchove and El Khoury, 2013) (Fig. 2). Several studies have described the geometry of the aortic root (Cheng et al., 2007; Dagum et al., 1999; Lansac et al., 2002), however few studies have described what forces act on the aortic root. This is imperative, since the forces acting on the aortic root will influence the function of the aortic valve and hence the longevity of the treatment. By combining measures of force and geometry, a measure of distensibility can be derived, yielding biomechanical information on the different segments of the native functional aortic annulus. Furthermore, the elastic energy stored in the aortic root can be estimated using a combination of geometrical data and the aortic blood pressure, and act as a surrogate measure of the compliance of the root. We hypothesize that such information can aid the surgeon in selecting the optimal repair strategy for each individual patient, in order to enhance the durability of the repair. Characterizing the behavior of the native aortic root could provide the surgeon with new information that enables prediction of areas that may require additional attention during surgery. An example could be a thinned aorta wall in a segment shown to exhibit increased mechanical stress compared to other segments. Furthermore, in-depth knowledge of the native aortic root provides a basis for developing new surgical techniques, which incorporates new knowledge regarding the behavior of the native aortic root.

* Corresponding author at: Department of Cardiothoracic and Vascular Surgery, Aarhus University Hospital, Palle Juul-Jensens Boulevard 99, 8200 Aarhus N, Denmark.

E-mail address: hasenkam@clin.au.dk (J.M. Hasenkam).

[1] Both authors contributed equally to this manuscript.

https://doi.org/10.1016/j.jbiomech.2018.04.037
0021-9290/© 2018 Elsevier Ltd. All rights reserved.

The aim of this study was therefore to establish a model for a characterization of the aortic root and use this model to investigate the native functional aortic annulus by measures of force and geometry, since these parameters can influence the function of the aortic valve. Such data from the native aortic root can be used as reference for examining the impact of surgical interventions on the aortic root. Furthermore, these data can also be beneficial when dealing with minimal invasive procedures such as transcatheter aortic valve replacement, where the expansion force of the valve can be related to the aortic root distensibility (Mummert et al., 2013).

2. Materials and Methods

2.1. Animal model

Ten female pigs (mixed Duroc and Danish Landrace) with an average bodyweight of 80 kg were used in this acute experimental study. The handling of the animals was conducted in compliance with the Danish law on animal experimentation, and the study was approved by the Danish Inspectorate of Animal Experimentation.

The transportation, medication, anesthesia, sternotomy and extracorporeal circulation in pigs at our institution have been previously described (Hasenkam et al., 1994; Nielsen et al., 2011). In the present study the animals received additionally 3.75 mg/kg Cordarone and 50.000 units of heparin during surgery.

In order to quantify the biomechanics of the aortic root, two force transducers (Bechsgaard et al., 2017) and eleven sonomicrometry crystals were implanted within each animal as illustrated in Fig. 2.

Following initiation of extracorporeal circulation and cardioplegic arrest, the annular force transducer was inserted through an apical incision and sutured to the interleaflet triangles just upstream of the aortic valve (Fig. 1A) using tourniquets. Three crystals were implanted one at each leaflet nadir and one in the left ventricular apex before closure of the apical incision using Prolene® 4–0 (Ethicon Inc., Somerville, New Jersey, USA).

The aortic valve was exposed through a transverse aortotomy approximately one cm downstream of the commissures, where sonomicrometry crystals were placed; one at each free edge of the cusp, one at each commissural point and one reference in the ascending aorta. Prior to closure of the ascending aorta, the second force transducer (STJ transducer) was placed extravascularly on the aorta with the three sensing rods proximal to the aortic valve at the commissural level (Fig. 1B).

The aorta was closed with Prolene 4–0 using a two-layer technique with a deep mattress suture and a superficial over-and-over suture. Following aortic closure, the three force arms of the STJ transducer were fastened to the commissural points and the transducer base was sutured to the ascending aorta using tourniquets. All sonomicrometry crystals were two mm in size (2 mm with dual suture loop, Sonometrics Corp., London, Ontario, Canada), secured using PremiCron® 2–0 (B. Braun, Melsungen, Germany). However, the three cusp crystals which were one mm (1 mm with single suture loop, Sonometrics Corp.,) and secured using Prolene 6–0 suture. Following implantation of force transducers and sonomicrometry crystals, mikro-Tip® blood pressure catheters were placed in both the left ventricle and the ascending aorta.

At the end of the experiment after data collection, each pig was euthanized during continued anesthesia by injecting an intravenous overdose of pentobarbital.

2.2. Data acquisition

Following successful implantation of the measuring equipment, reperfusion and weaning off bypass, the first data collection sequence was performed under hemodynamic stable conditions. The data collection comprised force, pressure and ECG data. Twenty seconds of data was obtained during each sampling session which was stored for offline analysis. Following the first data acquisition sequence, the tourniquets holding the force transducers were loosened to allow removal of both transducers. The annulus transducer was then pulled down into the left ventricle, and the STJ transducer was moved towards the aortic arch to allow for a second data collection without the force transducers interfering with sonomicrometry data collection. This transducer manipulation was performed during a short period extracorporeal circulation on beating heart. The second dataset was collected after hemodynamic stable conditions were reestablished. Two-

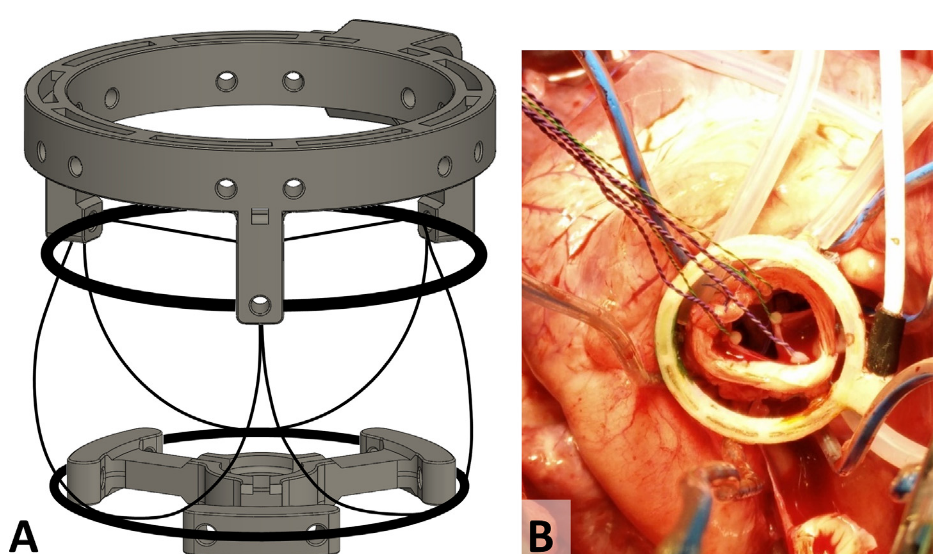

Fig. 1. (A) Schematic drawing of the aortic root and the placement of annular transducers (lower) and the STJ transducer (upper). (B) Picture showing the sinotubular junction transducer being implanted within a porcine aortic root. The small wires exiting the aorta are the lead wires for the sonomicrometry crystals. The annular transducer is not visible, but has been implanted upstream of the aortic valve.

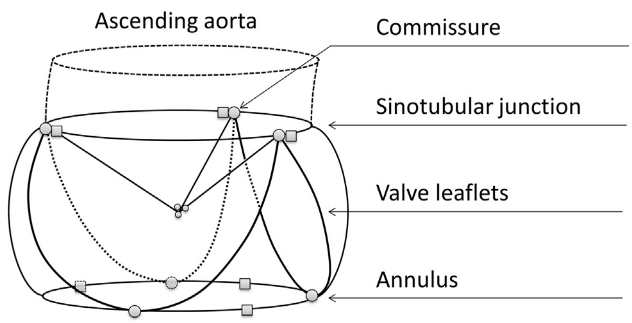

Fig. 2. Schematic presentation of the functional aortic root with sonomicrometry and force measurement positions. Circles indicate sonomicrometry crystals position and squares indicate where the force transducer arms were secured. At the sinotubular junction, the crystals and force transducer were placed in the same location. The reference crystals are not displayed in the figure.

dimensional echocardiography (Vivid I, GE Vingmed Ultrasound AS, Horten, Norway) was performed to verify valve competence at baseline, following transducer implantation, and after force transducer removal.

The ECG was amplified and monitored using a cardiomed system (Model 4008, CardioMed A/S, Oslo, Norway). The blood pressure was acquired using Mikro-Tip® catheters in conjunction with a signal conditioner (SPR-350 & PCU-2000, Millar Instruments).

The analog data (pressure, force and ECG) were all acquired with a sample rate of 1613 Hz using dedicated hardware and software (NI cDAQ 9172, NI 9237, NI 9215 and LabVIEW 2015, National Instruments, Austin Texas, USA). The sonomicrometry data was acquired with a sample rate of 297 Hz using the Sonometrics TRX USB transceiver system and the SonoLabDS3 acquisition software package (Sonometrics Corp.).

2.3. Data analysis

All data was post-processed and analyzed postoperatively offline. The first derivative of the left ventricular pressure (dP dt^{-1}) was used to derive and define identifying time stamps in the data. Early Systole was defined as dP dt^{-1} max and Early Diastole as dP dt^{-1} min.

The *Mid Systole* (Mid Sys) was defined as time center between dP dt^{-1} max and min, whereas *Mid Diastole* (Mid Dia) were between dP dt^{-1} min and max. The minimum and maximum time points were the amplitude minimum and maximum with respect to each single parameter reported.

Data is reported in two intervals; the first is Mid Sys-Mid Dia which is the change in amplitude from Mid Systole to Mid Diastole, and the second is MAX-MIN which is the change in amplitude from maximum to minimum.

The force reported are relative forces, which have been offset adjusted to yield zero N during diastole.

Data from the sonomicrometry system was further post-processed (SonoSOFT and SonoXYZ, Sonometrics Corp.). From these data, three circular sectors (segments, corresponding to the right-left, right-non and left-noncoronary) were calculated for both the annular level and the STJ level and were based on the three points obtained from each plane.

Since the STJ force measurements are in the same anatomical location as the crystals (commissures), the segment lengths of STJ were calculated as an average of two segments (Eq. (1)).

$$S_{est\ RightNon} = \frac{S_{Right} + S_{Non}}{2}, \tag{1}$$

This allowed us to compare the segments of STJ with the segments at the annular level (leaflet nadir), since these are separated by 60 degrees.

Based on the three crystals both at the annular level and at the STJ, the aortic root volume was calculated as a truncated cone. By plotting the aortic volume against the aortic pressure, a Pressure-Volume loop was created. The area contained within the Pressure-Volume loop is a measure of the elastic energy stored in the aortic root as a measure of overall root distensibility, calculated using the polygon function within MATLAB (polyarea, MATLAB 2016B, MathWorks, MA, USA).

To calculate the radial structural stiffness as a measure of the segmental compliance of the aortic root, the change in force was compared with the change in segment length at two time points for both the annular and STJ level. Between these time points, a straight line was plotted and the slope calculated (Eq. (2)) which was defined as the radial structural stiffness (RSS) of each segment.

$$\mathrm{RSS} = \frac{\boldsymbol{\Delta Force}}{\boldsymbol{\Delta Length}} = \frac{\boldsymbol{F_{Midsystole} - F_{Middiastole}}}{\boldsymbol{L_{Midsystole} - L_{Middiastole}}}, \tag{2}$$

2.4. Statistical analysis

Of the 20 s of data stored in each data collection cycle, ten consecutive heart cycles were identified and extracted based on the smallest variation in maximum left ventricular pressure. The statistical quantity reported within this manuscript is the mean (standard deviation) for all included animals.

The collected data was analyzed using a mixed model with nested random effects to take into account the repeated measurements on animal and anatomical location within animal levels. Following the mixed model, the residuals were inspected for normality and no reason to refute this was found. A p-value < 0.05 was defined as statistically significant. The data was analyzed using Stata 13.0 (StataCorp LLC, Texas, USA).

3. Results

Out of ten pigs, one was excluded due to force transducer malfunction and two could not be weaned from extracorporeal circulation, which left seven pigs to be included for analysis.

The data presented in this manuscript were collected under stable hemodynamic conditions as listed in Table 1.

The geometrical data was acquired in average 23 min (SD 9) after the force data recordings. There was a statistical difference in the aortic and transvalvular pressure between the dataset with and without force transducer implanted, as seen in Table 1. The waveforms in Fig. 3 illustrate the relationship between force and geometry data of the right and non-coronary annular segment from one representative animal.

It is seen from Fig. 3 that the force tracing was slightly delayed compared with the left ventricular pressure tracing (mean delay 35 ms (SD 24)). Such a delay was not found between the geometrical data and left ventricular pressure. An increase in force is closely correlated with an increase in left ventricular pressure and segment length as shown in Fig. 3. The segmental change in force of the annular and STJ plane is shown in Fig. 4. In the annular level, the right-left segment exhibited the largest cyclic force and it was statistically significant at both time intervals. In the STJ plane, the right-left segment exhibits the lowest cyclic force, however not statistically significant compared with the other segments.

The segmental change in length is shown in Fig. 5. In the annular level, the right-left segment exhibited a significantly smaller cyclic change in length compared with the other segments at both time intervals. In the STJ plane, all segments were similar and only

Table 1
Hemodynamic parameters with and without force transducer implanted reported as mean and SD. LVP: Left Ventricle Pressure, AP: Aortic Pressure, dP dt^{-1} max: maximum of the first derivative of left ventricular pressure. Data based on ten cycles from all included animals. In the group without force transducer, no cross-clamp was used during the removal of the implanted transducers.

	Heart rate (BPM)	LVP max (mmHg)	AP max (mmHg)	dP dt^{-1} max (mmHg s^{-1})	Transvalvular pressure (mmHg)	Cross-clamp time (min)
With force transducer	102.8 (SD 27.3)	89.5 (SD 8.9)	64.6 (SD 4.8)	1574.2 (SD 373.6)	31.4 (SD 6.7)	80.6 (SD 12.0)
Without force transducer	121.8 (SD 15.0)	89.9 (SD 19.6)	81.3 (SD 19.4)	1730.9 (SD 461.2)	18.4 (SD 7.7)	n/a n/a
P value	0.171	0.953	0.028	0.388	<0.001	n/a

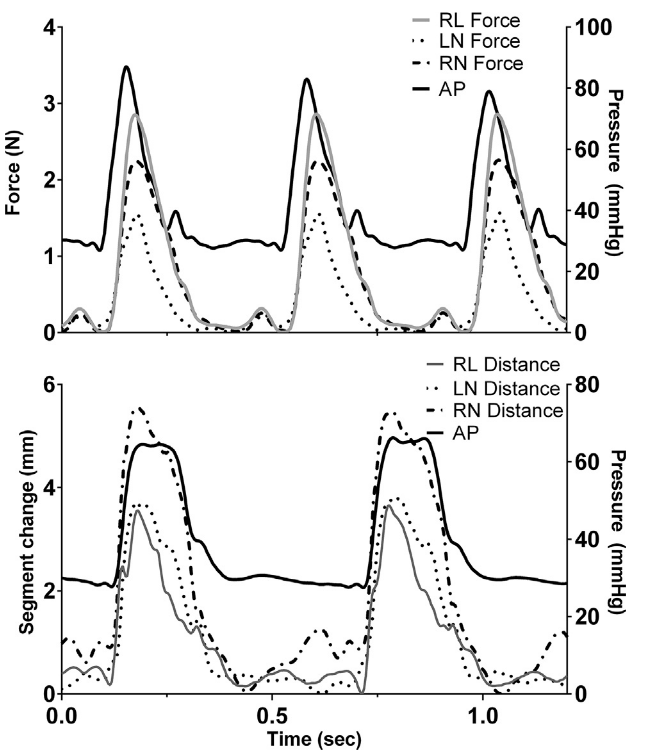

Fig. 3. Example of the relationship between force and segment length of one included animal. The two datasets were collected 19.5 min apart. AP: Aortic pressure, RL: right to left coronary, RN: right to non-coronary, LN: left to non-coronary.

statistically significant different between right-noncoronary and left-noncoronary at the Mid Sys-Mid Dia time interval.

The radial structural stiffness for all segments for both planes are shown in Fig. 6.

In the annular plane the right-left segment was statistically significantly stiffer than the two other segments, whereas the right-left segment was most compliant in the STJ level, however only significant between right-left and right-noncoronary at the Mid Sys-Mid Dia time interval. A table summarizing the data is shown in Table 2.

An example of a pressure–volume loop is shown in Fig. 7. One animal was excluded from these calculations, due to erroneous aortic pressure data. The volume and elastic energy was calculated based on the remaining six pigs. The average aortic root volume was 4.62 mL (SD 0.41) and the group-mean elastic energy was 882 μJ (SD 552).

4. Discussion

This study is the first to measure segmental forces of the aortic root and combine these with the segmental changes in geometry, to obtain an expression of the compliance of each segment within the aortic root.

At both the Max-Min and Mid Sys-Mid Dia time intervals, the maximum force in the annular plane was in the right-left segment, which corresponds to the muscular segment of the aortic annulus (Komiya, 2015). The minimum force was found in the right-non-coronary segment, which includes the fibrous segment that anchors the anterior leaflet of the mitral valve. At the STJ level, the maximum force was in the right-non-coronary segment, whereas the minimum force was in the right-left segment. None of the force segments within the STJ were statistically significant different.

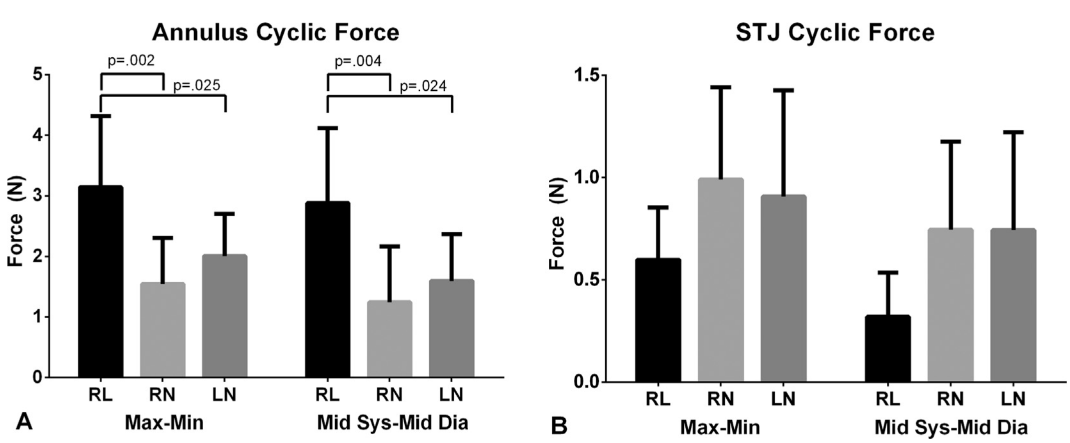

Fig. 4. Cyclic force distribution in (A) Annular plane and (B) Sinotubular junction (STJ). At the annular level the cyclic force is most pronounced greatest in the RL segment at both time intervals. At the level of the STJ, the RN segment has the largest mean change at both time intervals, however not statistically significant compared with the other segments. RL: right to left coronary, RN: right to non-coronary, LN: left to non-coronary.

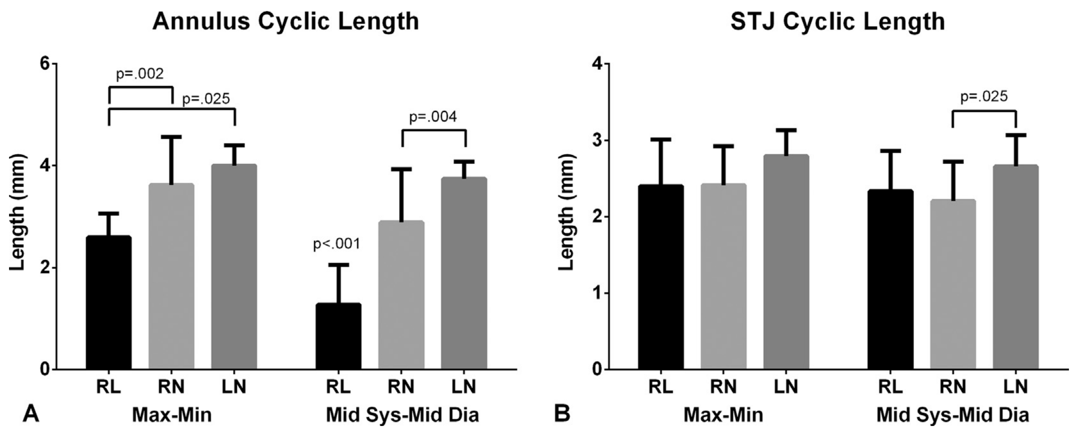

Fig. 5. Cyclic change in segment length in (A) Annular plane and (B) Sinotubular junction (STJ). At the Mid Sys-Mid Dia time interval at the annular level, all segments are statistically significant different at the Mid Sys-Mid Dia time interval. The LN segment has the largest change at both time points, however only statistically significant different at the Mid Sys-Mid Dia time interval. (B) At the STJ, the same tendency is seen, however only statistically significant different between the RN and LN at the Mid Sys-Mid Dia time interval. RL: right to left coronary, RN: right to non-coronary, LN: left to non-coronary.

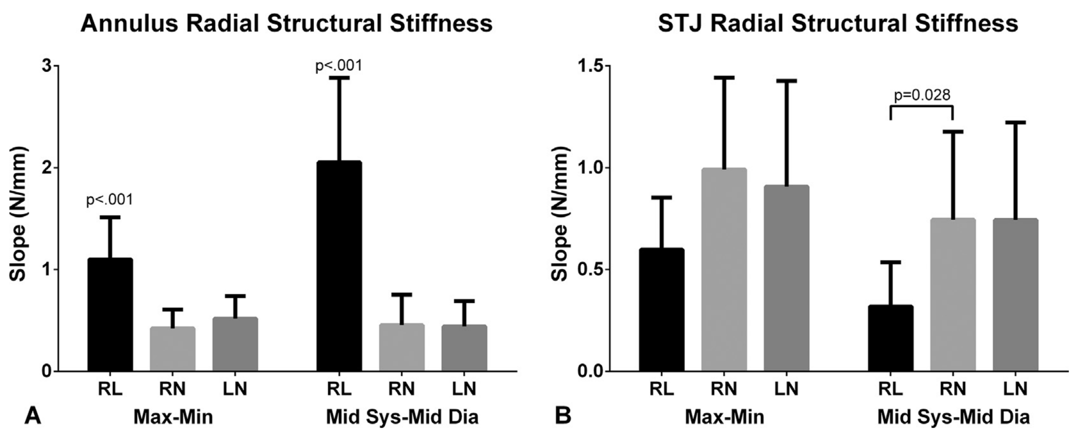

Fig. 6. Force-length relationship for (A) the annular plane and (B) the sinotubular junction (STJ). A high value indicates a low apparent elasticity, as it requires a larger force to distend the same length. RL: right to left coronary, RN: right to non-coronary, LN: left to non-coronary.

Table 2
Summarizing table, data shown is mean and SD based on ten cycles from each included animals (n = 7).

Time point	Mid systole - mid diastole			Maximum - minimum		
Segment	Right to left	Left to noncoronary	Noncoronary to right	Right to left	Left to noncoronary	Noncoronary to right
Annulus force (N)	2.88 (SD 1.23)	1.59 (SD 0.76)	1.24 (SD 0.92)	3.14 (SD 1.17)	2.00 (SD 0.69)	1.54 (SD 0.76)
STJ force (N)	0.32 (SD 0.22)	0.74 (SD 0.48)	0.74 (SD 0.43)	0.59 (SD 0.25)	0.91 (SD 0.52)	0.99 (SD 0.45)
Annulus geometry change (mm)	1.27 (SD 0.78)	3.74 (SD 0.34)	2.88 (SD 1.05)	2.59 (SD 0.47)	4.00 (SD 0.40)	3.62 (SD 0.94)
STJ geometry change (mm)	2.34 (SD 0.53)	2.66 (SD 0.41)	2.20 (SD 0.52)	2.40 (SD 0.61)	2.79 (SD 0.34)	2.41 (SD 0.51)
Annulus segmental radial stiffness (N/mm)	2.05 (SD 0.82)	0.44 (SD 0.25)	0.45 (SD 0.30)	1.1 (SD 0.41)	0.52 (SD 0.22)	0.42 (SD 0.18)
STJ segmental radial stiffness (N/mm)	0.32 (SD 0.22)	0.74 (SD 0.47)	0.74 (SD 0.43)	0.60 (SD 0.26)	0.90 (SD 0.52)	0.99 (SD 0.45)

The change in shape for the aortic root has been described as a circular configuration in systole to an oval configuration in diastole (De Heer et al., 2011; Suchá et al., 2015). Such a shape change may cause the forces at different segments to be uneven, since the root most likely will exert the greatest force in the long axis of the oval shape. This does not necessarily mean that the maximum force segment also has the most prominent change in length since this depends on the structural tissue composition. Though it is expected to be homogeneous at the STJ level, it is not the case in the annular level since it is composed of different kinds of tissue such as muscular and fibrous tissue (Anderson, 2007).

The pressure has been described as being the governing quantity (Cheng et al., 2007), that closely correlates with a change in geometry. The force transducers utilize strain gauges to detect a deformation of a spring element, which makes them primarily sensitive to a change in geometry. Hence, a change in pressure will cause a change in geometry that will lead to a change in force amplitude.

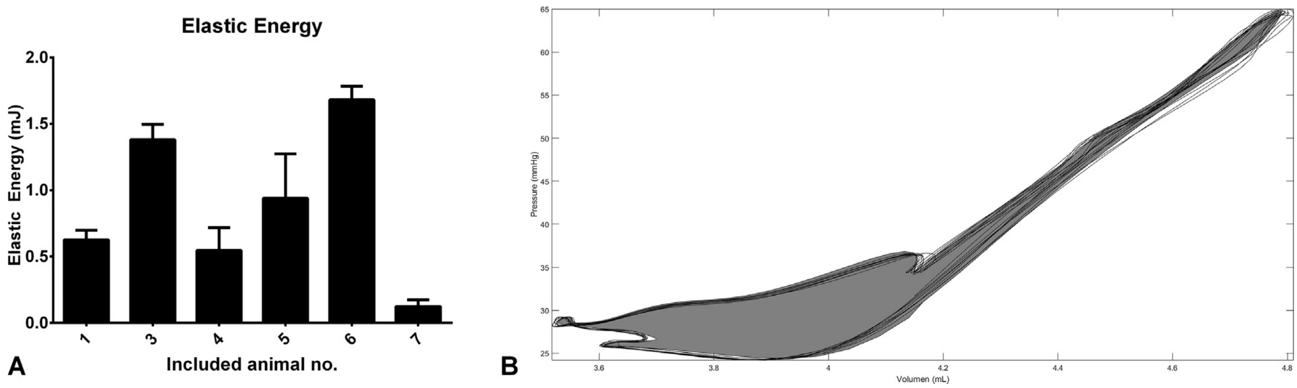

Fig. 7. (A) The elastic energy storage for the six included animals. (B) A representative plot of the nine cardiac cycles comprising the aortic root pressure-volume relationship. The work performed in this PV loop is the elastic energy stored in the aortic root. In the current graph, the area of a single cardiac cycle is colored and the mean elastic energy for all cycles was 624 μJ (SD72).

The left-noncoronary segment exhibited the most pronounced geometrical change for both the annular level and the STJ (Fig. 5). This location coincides with the segment reported to be most prone to dilation which is the noncoronary sinus (Cotrufo et al., 2003). The change in right-left annular segment length was in all cases statistically significantly smaller compared with the other two segments. An explanation could be that the right cusp has a wide muscular shelf (Schäfers, 2012), and a contraction of this segment could minimize the systolic flow-induced dilatation that occurs due to blood being ejected from the left ventricle. Hence, the total change in length is minimized and the segment can be interpreted as more restrictive. The same explanation can be applied for the other two segments in the annular level, since the right-noncoronary segment is reported to contain partly muscle and fibrous tissue (Komiya, 2015), and only exhibits miniscule change in segment length. The last segment, which is the left-noncoronary, is reported to only contain fibrous tissue and thereby does not have a contracting element, nonetheless the largest change in length is seen in this segment.

The cyclic segment length in the STJ plane was almost equal and only significantly different between left-noncoronary and right-noncoronary at the Mid Sys-Mid Dia time interval. This supports the previously stated hypothesis that the STJ tissue is homogeneous and the forces are governed by the volume displacement within the aortic root. At the annular level, there was no statistically significant difference between the radial structural stiffness in the right-noncoronary and left-noncoronary segments at either time interval. However, the right-left segment is significantly stiffer than the two other segments, it also coincides with the muscular part of the annulus as stated above.

At the STJ level, the opposite seems to be the case since the right-left segment seems more compliant than the two other segments, however only statistically significant different between the right-left and right-noncoronary segment at the Mid Sys-Mid Dia time interval. The radial structural stiffness was calculated from the segmental force and geometry data and yields information about the local change in the aortic root, it is susceptive to both a change in force and geometry which can be seen from the presented data. The aortic root elastic energy is based on measures derived from sonomicrometry crystal distances from the annular plane to the STJ plane of the aortic root. Therefore, it is restricted to provide information about the aortic root alone and not the entire aortic section, even though the sections are interconnected. The elastic energy is an expression of the overall aortic root compliance, and is established to form a baseline that can be used for investigation of different surgical repair procedures for the aortic root.

The forces measured in this study are based on deformations acting on the strain measuring transducer. Through the calibration procedures these strains are converted into the resulting radial forces (Bechsgaard et al., 2017). The way of describing aortic root forces in a unidirectional scheme provides a rather simplified picture since the aortic root experiences both radial, longitudinal, torsional, and shear deformations (Cheng et al., 2007). However, for an experimental approach we believe that measuring unidirectional forces by acquiring the radial force components provides an important parameter for describing the aortic root dynamics. A small delay was observed between the left ventricular pressure and the forces in both the annular and the STJ level in all pigs. The blood pressure can increase very rapidly, however the flow cannot increase simultaneously which can be explained by the blood inertia and momentum (Oates, 2008) as well as viscous effects. Since the force transducer is sensitive to a change in volume only, a small time delay is introduced between the pressure and force data tracings. Since this delay in force signal could impact the data readout of specific time points i.e. Mid Sys-Mid Dia, a minimum and maximum point was found for each parameter for each heart cycle. This approach allows for a comparison between the extreme values, which are independent of time within each cardiac cycle, hereby eliminating the effect of a time delay between the recorded signals. The described biomechanical model aids to identify segments which may require special attention during surgical interventions. This could be using felt-pledges in segments with high force amplitudes or adding support at segments with large deformations. Furthermore, the data acquired using the described model can aid in refining existing surgical techniques for the aortic root.

5. Limitations

A sample size in the present study of n = 7 (n = 6 for the PV-loop data), could be argued to be too few to assume normal distribution, however the statistical model validation performed did not give rise to doubt this assumption. Since this study was performed in an acute porcine model, care should be taken to extrapolate the absolute force and length values to human conditions. Furthermore, the porcine model used in this study was healthy and hence does not mimic pathological conditions. This model, however, still allows investigation on how the different surgical manipulation affects the normal aortic root. It is expected that these results can be used to improve surgical procedures currently used to treat patients.

Out of a total of 21 force recordings from the annular force transducer, two were discarded due to malfunctioning strain gauges. The discarded data was replaced with segment means from all included data, using the mean imputation method. Furthermore, since the strain gauges are all in the same plane and not completely perpendicular on the transducer sensing elements, crosstalk between stain gauges will be introduced. This can result in ambiguous force measurements in the three segments.

During the data analysis of the geometrical data, some sonomicrometry distances were erroneous and therefore excluded. The distances between crystals in the same plane were evaluated, and if some were larger than the diameter of the aortic root, they were replaced with an estimate based on the remaining trustworthy distances. This was done with six segments in the annular plane and two in the STJ plane out of a total of 42 segments.

As the force and sonomicrometry data have been collected about 23 min apart, the contractility of the heart could have changed, leading to a possible mismatch. However, parallel recording of these data was not feasible since implanting of the force transducers stiffens the aortic root thus limiting the geometrical change of the root and thereby underestimating the actual changes in distances. Nonetheless, no significant difference in contractility (dP dt^{-1}) was found between the datasets with and without force transducer implanted. There was a statistically significant difference in the transvalvular- and aortic pressure with and without the force transducers implanted. This could influence the amplitude of the forces measured in the STJ, however the impact is equal to all force segments measured hereby eliminating a direct impact on the comparisons between segments.

The results presented in this paper are translational for comparison in similar studies on both same and different size aortic roots as well as pathological aortic roots. The absolute force measurements are susceptible to variations in future studies with change in transducer materials and geometries, which is the circumvented by introducing the local structural stiffness as an invariant measure.

6. Conclusion

We have successfully created a model for the investigation of the biomechanics of the aortic root in pigs. We have identified obvious differences in the segmental force and geometry between the aortic annulus and the sino-tubular junction. These data have been combined to obtain an expression of the compliance of each segment within the aortic root, which has not been done before. Such measurements of the native porcine model is reference for future studies, investigating different types of surgical techniques for the aortic root.

Acknowledgement

The project was funded by The Danish Heart Foundation Grant #15-R99-A5942-22906, The Danish Council for Independent Research Grant #DFF-4004-00317, Aarhus University, Direktør Jacob Madsens & Hustru Olga Madsens Fond, Direktør Kurt Bønnelycke og hustru fru Grethe Bønnelyckes Fond, Edith og Olfert Dines Hansens Legat, Helga og Peter Kornings fond, Holger Rabitz og hustru Doris Mary født Philipp's Mindefond, Snedkermester Sophus Jacobsen og hustru Astrid Jacobsens Fond, Karen Elise Jensens Fond.

None of the sponsors were actively involved in the study design, data collection/analysis or the writing of this manuscript.

Conflict of interest

None of the authors have any conflicts of interest to declare.

Footnotes

No human studies were carried out by the authors for this article.

The handling of the animal in this experiment was conducted in compliance with the Danish law on animal experimentation and the study was approved by the Danish Inspectorate of Animal Experimentation.

References

Anderson, R.H., 2007. The surgical anatomy of the aortic root. Multimed. Man. Cardiothorac. Surg. 2007 (102). https://doi.org/10.1510/mmcts.2006.002527.
Bechsgaard, T., Honge, J.L., Nygaard, H., Nielsen, S.L., Johansen, P., 2017. Biomechanical assessment of the aortic root using novel force transducers. J. Biomech. 61, 58–64.
Boodhwani, M., El Khoury, G., 2014. Aortic valve repair: Indications and outcomes. Curr. Cardiol. Rep. 16 (490), 1–6.
Cheng, A., Dagum, P., Miller, D.C., 2007. Aortic root dynamics and surgery: from craft to science. Philos. Trans. R. Soc. Lond. B. Biol. Sci. 362, 1407–1419.
Cotrufo, M., Corte, A. Della, Santo, L.S. De, Feo, M. De, Covino, F.E., 2001. Asymmetric medial degeneration of the ascending aorta in aortic valve disease: a pilot study of surgical management. Int. J. Card. 81, 37–41.
Dagum, P., Green, G.R., Nistal, F.J., Daughters, G.T., Timek, T.A., Foppiano, L.E., Bolger, A.F., Ingels, N.B., Miller, D.C., 1999. Deformational dynamics of the aortic root : modes and physiologic determinants. Circulation 100. II-54-II-62.
David, T.E., Feindel, C.M., 1992. An aortic-valve sparing operation for patients with aortic incompetence and aneurysm of the ascending aorta. J. Thorac. Cardiovasc. Surg. 103, 617–622.
De Heer, L.M., Budde, R.P.J., Mali, W.P.T.M., De Vos, A.M., Van Herwerden, L.A., Kluin, J., 2011. Aortic root dimension changes during systole and diastole: Evaluation with ECG-gated multidetector row computed tomography. Int. J. Cardiovasc. Imaging 27, 1195–1204.
de Kerchove, L., El Khoury, G., 2013. Anatomy and pathophysiology of the ventriculo-aortic junction: implication in aortic valve repair surgery. Ann. Cardiothorac. Surg. 2, 57–64.
Hasenkam, J.M., Nygaard, H., Paulsen, P.K., Kim, W.Y., Hansen, O.K., 1994. What force can the myocardium generate on a prosthetic mitral valve ring? An animal experimental study. J. Heart Valve Dis.
Komiya, T., 2015. Aortic valve repair update. Gen. Thorac. Cardiovasc. Surg. 63, 309–319.
Lansac, E., Lim, H.S., Shomura, Y., Lim, K.H., Rice, N.T., Goetz, W., Acar, C., Duran, C.M.G., 2002. A four-dimensional study of the aortic root dynamics. Eur. J. Cardiothorac. Surg. 22, 497–503.
Mummert, J., Sirois, E., Sun, W., 2013. Quantification of biomechanical interaction of transcatheter aortic valve stent deployed in porcine and ovine hearts. Ann. Biomed. Eng. 41, 577–586.
Nielsen, S.L., Lomholt, M., Johansen, P., Hansen, S.B., Andersen, N.T., Hasenkam, J.M., 2011. Mitral ring annuloplasty relieves tension of the secondary but not primary chordae tendineae in the anterior mitral leaflet. J. Thorac. Cardiovasc. Surg. 141, 732–737.
Oates, C., 2008. Cardiovascular haemodynamics and Doppler waveforms explained. Cambridge University Press, Cambridge.
Sarsam, M.A.I., Yacoub, M., 1993. Remodeling of the aortic-valve anulus. J. Thorac. Cardiovasc. Surg. 105, 435–438.
Schäfers, H.J., 2012. Aortic annuloplasty: A new aspect of aortic valve repair. Eur. J. Cardio-thoracic Surg. 41, 1124–1125.
Suchá, D., Tuncay, V., Prakken, N.H.J., Leiner, T., Van Ooijen, P.M.A., Oudkerk, M., Budde, R.P.J., 2015. Does the aortic annulus undergo conformational change throughout the cardiac cycle? A systematic review. Eur. Heart J. Cardiovasc. Imaging 16, 1307–1317.